24th U.S. Symposium
on Rock Mechanics
June 1983

NUMERICAL STUDIES OF LABORATORY TRIAXIAL CREEP TESTS*

LINDA J. BRANSTETTER
DALE S. PREECE
Applied Mechanics Division I
Sandia National Laboratories
Albuquerque, NM 87185

ABSTRACT

Triaxial creep experiments conducted on cylindrical specimens provide the basic data for modeling the behavior of rock salt. Even in the most carefully performed of these experiments, frictional effects between the ends of the salt sample and the platens of the testing machine prevent homogeneous stress and strain conditions from being achieved. Using the finite element technique, detailed analyses of uniaxial and triaxial creep experiments are performed to investigate the extent of the inhomogeneities caused by end effects. It is then possible to estimate the errors which the end effects produce in the interpretation of creep data on rock salt.

INTRODUCTION

In recent years underground storage programs have been proposed for placing nuclear wastes and hydrocarbons in salt formations. Examples of this are the Waste Isolation Pilot Plant (WIPP) which is envisioned to be a demonstration facility for the disposal of high level nuclear wastes in bedded rock salt in Southeastern New Mexico, and the U. S. Strategic Petroleum Reserves (SPR) which is to provide for the storage of crude oil in caverns leached in salt domes around the Gulf of Mexico. Design calculations for these programs rely on material descriptions which are determined from laboratory triaxial creep experiments on cylindrical specimens (Wawersik, 1980).

In deriving material models from the experimental data, the stress and strain state in the specimen is usually assumed to be homogeneous. For non-creeping triaxial test specimens the reasonableness of this assumption has been established by finite element simulations (Brady, 1973 and Baligh, 19731 and closed form solutions (Peng, 1971). These investigations have explored the effects of specimen geometry, end cap stiffness, and friction between the end cap and the sample. All of these investigations employed linear elasticity to model the behavior of the non-creeping rock specimen.

The nonlinearities associated with a creeping rock salt specimen greatly compound the problem of establishing the degree of uniformity of the stress and strain state within the specimen. Apparently this problem was first addressed by Wawersik and Preece (1981) who investigated the influence of end friction in a triaxial creep test. They employed the finite element program ADINA and modeled the friction force as a concentrated nodal load parallel to the salt/steel interface. The steel platen was not included in this analysis but was simulated by constraining the nodes at the end of the salt to always have the same axial displacement.

* This work was performed at Sandia National Laboratories supported by the U. S. Department of Energy under Contract Number DE-AC0476-DP00789.

This paper presents the results of new finite element simulations of two types of creep tests, one with radial pressure applied (called "confined") and the other with no radial pressure ("unconfined"). The finite element program used is a developmental code which uses the technique of dynamic relaxation to obtain solutions. The code also contains a slip plane capability. This makes it possible to include the steel end platen in the analysis with a frictional sliding interface between the steel and the salt. The predicted axial strain will be compared with the input creep model to determine the influence of end friction on the results. Several numerical exercises will be discussed that are necessary to separate numerical and physical phenomena. The predicted axial strain distributions within the simulated test specimens will be presented. The predicted average axial strain and axial strain rate will be compared to that predicted by a creep model derived from actual laboratory tests.

PROBLEM DESCRIPTION

Finite Element Model

Figure la shows the finite element representation used for all of the unconfined uniaxial test simulations. The model consists of a cylindrical salt specimen subjected to an axial stress which is transmitted through a massive steel platen or end cap. The left-hand boundary is the axis of rotation on which the shear stress and horizontal displacement are zero. A plane of symmetry exists at the specimen midheight, which is the lower boundary of the finite element model. This symmetry plane has zero shear stress and zero vertical displacement. The basic arrangement of Figure la was modified slightly in two cases: in the first, the end cap was removed so that the 5000 psi axial stress was applied directly to the salt; in the second, the axial compressive stress was distributed

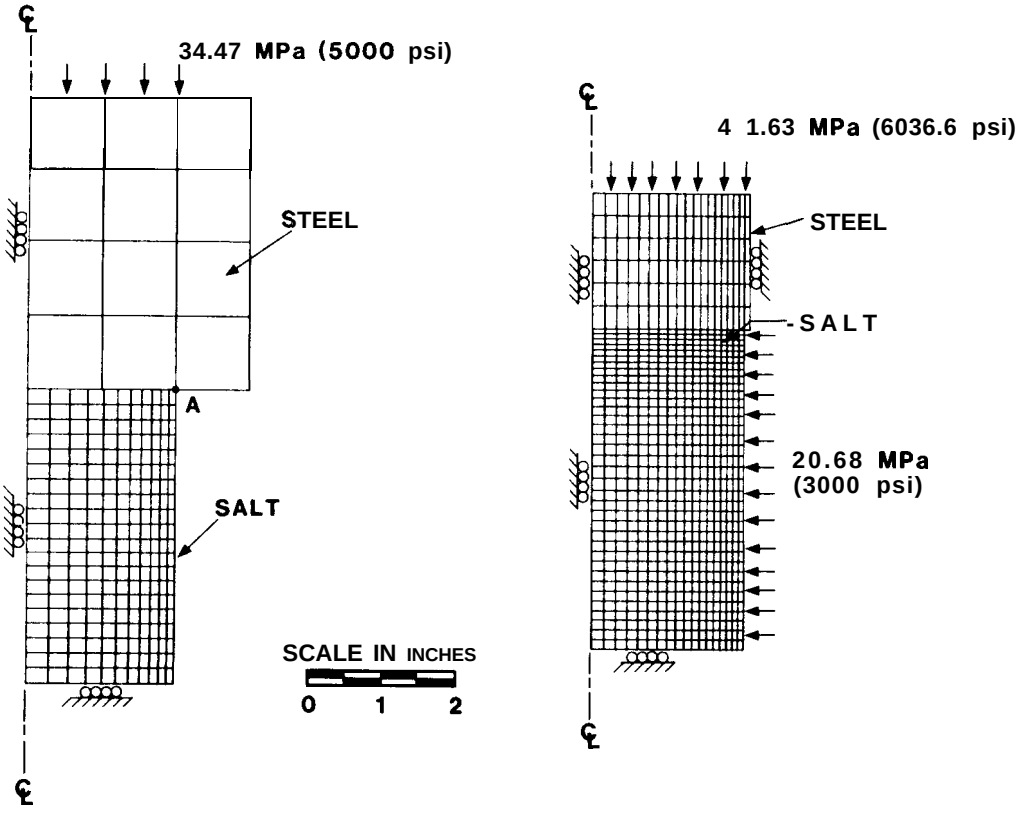

Figure 1. Axisymmetric Finite Element Models of Uniaxial and Triaxial Creep Test Specimens.

uniformly over the entire top area of the end cap. The stress in this case was reduced to 2222.2 psi, so that the resultant force transmitted to the salt specimen was the same for all unconfined test simulations.

Only one confined triaxial test is simulated in this study. The finite element representation of this experiment is shown in Figure lb. For this analysis, an axial compressive stress of 6038.6 psi was applied uniformly over the upper end cap surface. This resulted in an applied average vertical stress of 6500 psi on the salt specimen. The specimen was also subjected to a constant lateral pressure of 3000 psi.

Note that in both models the steel end cap extends radially beyond the salt to allow the salt to creep outward along the surface of the steel. A Mohr-Coulomb model was used to specify the interfacial friction.

Force Update Procedure

Considerable variation in the cross-sectional area of the specimen can occur as it undergoes creep deformation. A simple procedure based on incompressibility and constant volume strains has been used by experimenters in triaxial testing to compensate for the area variation in order to maintain constant average axial stress on the deforming specimen (Wawersik and Preece,1981). The effective change in cross-sectional area of the specimen at any time may be measured exactly where the diameter increase is some "average" value. This location may shift with time as the specimen barrels due to friction at the interface between the specimen and the end cap.

A lower bound estimate of the change in specimen area is obtained at the interface between the specimen and the end cap. It is here that frictional end effects and the resulting restraint to radial deformation are largest. An upper bound estimate of the change in specimen area is obtained at the specimen midheight (the lower boundary of these finite element test simulations) where end effects are minimized and the radial deformation is largest. Monitoring diameter change along the length of a jacketed specimen is difficult to do experimentally. One experimental procedure that is often used to estimate area change is to monitor the relative axial displacement between the upper and lower platens of the test machine, and estimate an average deformed sample diameter using the assumptions of constant sample volume and straight sample sides (Wawersik and Preece, 1981). This area estimate falls intermediate between the two extremes of the specimen end and midheight values. For perfect interfacial slip, this method will exactly duplicate the theoretically required force update. For realistic values of the interfacial friction coefficient, some small error is inherent.

This particular force update procedure was incorporated into the finite element test simulations. The axial displacement of point "A" within the salt (refer to Figure la) was monitored throughout the finite element solution and used to compute the logarithmic axial strain by the following relation (Wawersik and Preece, 1981):

$$\varepsilon = -\ln\left(1 - \frac{\Delta \ell}{\ell}\right) \qquad (1)$$

where,

ε = logarithmic axial strain

ΔL = change in salt specimen half-height (the full height of the modeled half-specimen)

ℓ = original specimen half-height

The vertical applied stress was multiplied by one plus the logarithmic axial strain at the end of each converged time step in the finite element solution.

Creep Model and Material Properties

An elastic secondary creep model was used in the finite element solution. The model results from a large number of tests on salt samples similar to those simulated here, and is used in finite element calculations performed for the WIPP and SPR programs (Weart, 1981). The model relates the effective secondary creep strain rate to the effective stress in the following temperature-dependent manner:

$$\dot{\bar{\varepsilon}} = D \exp(-Q/RT)\, \bar{\sigma}^N \qquad (2)$$

where,

D = material constant

N = material constant

Q = thermal activation energy

$\dot{\bar{\varepsilon}}$ = effective secondary creep strain rate

$\bar{\sigma}$ = effective stress

R = universal gas constant

T = temperature, absolute scale

The creep equation may be more simply written as

$$\dot{\bar{\epsilon}} = A\,\bar{\sigma}^{N} \qquad (3)$$

where,

$$A = D \exp(-Q/RT)$$

A temperature of 88°F (304°K) was assumed for the unconfined test simulations. This is near the in situ temperature experienced by salt at depths of interest for the WIPP and SPR programs. Room temperature (72°F or 295°K) was assumed for the confined test. Using the material properties for salt contained in Table I, with the appropriate temperatures, the coefficient A for the unconfined tests was $8.7791E\text{-}26\ sec^{-1}\ psi^{-4.9}$, while that for the confined test was $1.111E\text{-}20\ sec^{-1}\ psi^{-4.9}$. The material properties used for the steel platen for the unconfined and confined tests are included in Table 1. Both sets of steel properties are typical values for commonly available steels.

It is necessary to relate the effective secondary creep strain rate to the directly measurable value of specimen average axial strain, el. The axial strain rate was determined from laboratory tests to be approximately equal to two thirds of the secondary shear strain rate (Herrmann, 19801, if conditions of incompressiblilty (Malvern, 1969, p. 364) are assumed. Making the appropriate substitutions into Equation 3 and integrating,

$$e_1 = A\,\bar{\sigma}^{N}\,t \qquad (4)$$

where t is time in seconds. The effective stress is the difference between the axial and radial stresses in a triaxial test, and the effective strain rate is equal to the axial strain rate. Equation 4 is the exact result which all of the finite element test simulations will be compared to.

TABLE I

Salt Elastic Properties

Analysis	E (psi)	E (G Pa)	ν
Unconfined	4.48×10^{6}	31.0	.25
confined	3.60×10^{6}	24.8	.25

Salt Creep Properties

Analysis	D	N	Q	A
unconfined	$5.79 \times 10^{-36}\ Pa^{-4.9}\ sec^{-1}$	4.9	12 kcal/mole	$1.37 \times 10^{-44}\ Pa^{-4.9}\ sec^{-1}$
	$(3.72 \times 10^{-17}\ psi^{-4.9}\ sec^{-1})$			$(8.78 \times 10^{-26}\ psi^{-4.9}\ sec^{-1})$
confined	$8.64 \times 10^{-15}\ psi^{-4.9}\ sec^{-1}$	"	"	$1.11 \times 10^{-20}\ psi^{-4.9}\ sec^{-1}$
	$(1.34 \times 10^{33}\ Pa^{-4.9}\ sec^{-1}$			$(1.725 \times 10^{-39}\ Pa^{-4.9}\ sec^{-1})$
				(Weart, 1981)

Steel Elastic Properties

Analysis	E (psi)	E (G Pa)	ν
Unconfined	30.0 x 106	206.0	.30
confined	"	"	.27

Description of Analyses

A summary of seven test simulations is contained in Table II. The seven analyses simulate six unconfined tests (numbered 1 through 6 in Table II) and a single confined test (number 7 in Table II). The unconfined tests form a parametric study with the primary goal of evaluating inhomogeneities induced by end friction. From the work of Baligh (1973) on hard rock test simulations, end effects of varying degrees may be caused by several factors. Interfacial friction was identified as the major contributor. Other factors were the slenderness ratio of the simulated samples, Poisson's ratio of the tested material, stiffness of the end cap, and the manner in which the end cap was loaded. The unconfined test simulations of Table II were all performed with the same specimen geometry, so that slenderness effects were not investigated. The material properties of the simulated salt and end cap were the same for all unconfined tests. Thus, variations in Poisson's ratio of the salt and stiffness of the end cap were also not addressed here. The effect of loading method on the end cap was addressed in one of the unconfined simulations, as well as the effect of interfacial friction ranging from perfect slip to complete bonding. An intermediate friction value of 0.15 simulated a laboratory measured value for the interface derived from torsion tests (Wawersik and Preece, 1981).

The axial strain predicted in the simulations also depends on certain numerical parameters. The finite element mesh size must be fine enough to avoid predicted behavior which is unrealistically stiff. The mesh size used for the unconfined simulations in Table II was shown to be adequate through mesh refinement studies not included in this presentation. An equilibrium convergence tolerance used in the finite element solution was adjusted in one simulation to determine its effect. Not shown in Table II is a simulation which was identical to the second unconfined simulation, except that the end cap pressure was applied as in all of the other tests; that is, 5000 psi over the reduced cap top area as shown in Figure 1a. This simulation allows separation for comparison of the effects of the increased top area loading and different convergence tolerance used in Simulations 2 and 3. Results of this simulation are virtually identical to the results of Simulation 2, and will be described in the text. It will be referred to as Simulation 2' for convenience. The parametric study on the unconfined tests also isolated the effect of the force update procedure on the predicted behavior for a case with complete interfacial bonding.

The seventh simulation was the only confined example. The coefficient of friction between the specimen and end cap was 0.15 as in the sixth unconfined simulation. The convergence tolerance was set equal to 0.5 for very small axial strains, but was then

TABLE II

SIMULATION	PLATEN ?	PRESSURE/RADIUS	INTERFACE FRICTION COEFFICIENT	CONVERGENCE TOLERANCE (PERCENT)	FORCE UPDATE ?
1	no	5000 psi/2 in	N/A	0.5	N/A
2	yes	2222.2 psi/3 in	0.	0.5	yes
3	yes	5000 psi/2 in	0.	0.3	yes
4	yes	5000 psi/2 in	1. (fixed)	0.5	yes
5	yes	5000 psi/2 in	1. (fixed)	0.5	no
6	yes	5000 psi/2 in	0.15*	0.5	yes
7	yes	σ_1 = 6500 in σ_2 = 3000 psi	0.15*	0.5 to 1.3	yes

*Obtained from laboratory tests by Wolfgang R. Wawersik (Wawersik and Preece, 1981)

increased at larger strain values because of numerical difficulties. This is discussed later in the paper.

"SMALL" STRAIN ANALYSES OF UNCONFINED TEST SIMULATIONS

The unconfined simulations were all carried out to nominal axial strains on the order of ten percent. The axial strain histories predicted by these analyses are compared to the constitutive prediction of Equation 4 in Figure 2. Clearly the finite element solutions underpredicted the creep model in every case. Simulation 1, in which the salt is loaded directly, should have a homogeneous stress and strain field and should match the creep model exactly. At 8 days, the theoretical nominal axial strain from Equation 4 is 0.0809. The strain predicted by Simulation 1 lies 3.45 percent below that of the creep model, at a value of 0.0781. This deviation will be discussed with the results of some other simulations. A contour plot of axial strain in this simulated specimen at 8 days appears in Figure 3a, and shows that some nonuniformity of axial strain does exist. This is not as obvious in Figures 4 and 5, where axial strain at 8 days is plotted as a function of distance along the specimen axis and surface, respectively.

Two parameters were varied in Simulations 2 and 3, namely, the loaded top area of the end cap and the equilibrium convergence tolerance used in the finite element solution. One other simulation very similar to these was performed which will be referred to as Simulation 2'. Simulation 2' was identical to Simulation 2 except that the end cap was loaded identically to the other unconfined test simulations. Simulation 2' does not appear explicitly in Table II or any of the following figures since the results of that simulation were only slightly different from that of Simulation 2. The importance of Simulation 2' lies in the fact that it allows diffinitive separation of the effects of convergence tolerance, the presence of the end cap and the manner in which it is loaded.

The presence of the steel platen had a definite influence on the predicted axial strain behavior. Due to a discontinuity induced by the edge of the salt on the steel end platen (at the location of point "A" in the finite element solution), the results of Simulation 2' are not expected to match those of Simulation 1 exactly. A comparison of Simulation 1 and Simulation 2' shows that with the end cap, the percentage reduction in average axial strain from the creep model increased by 5.8 percent. The alternate method of loading the end cap (Simulation 2) causes only slight differences. Average axial strain in Simulation 2 is 8.59 percent below the creep model at 8 days, while Simulation 2' is 9.23 percent below the model. The 8 day

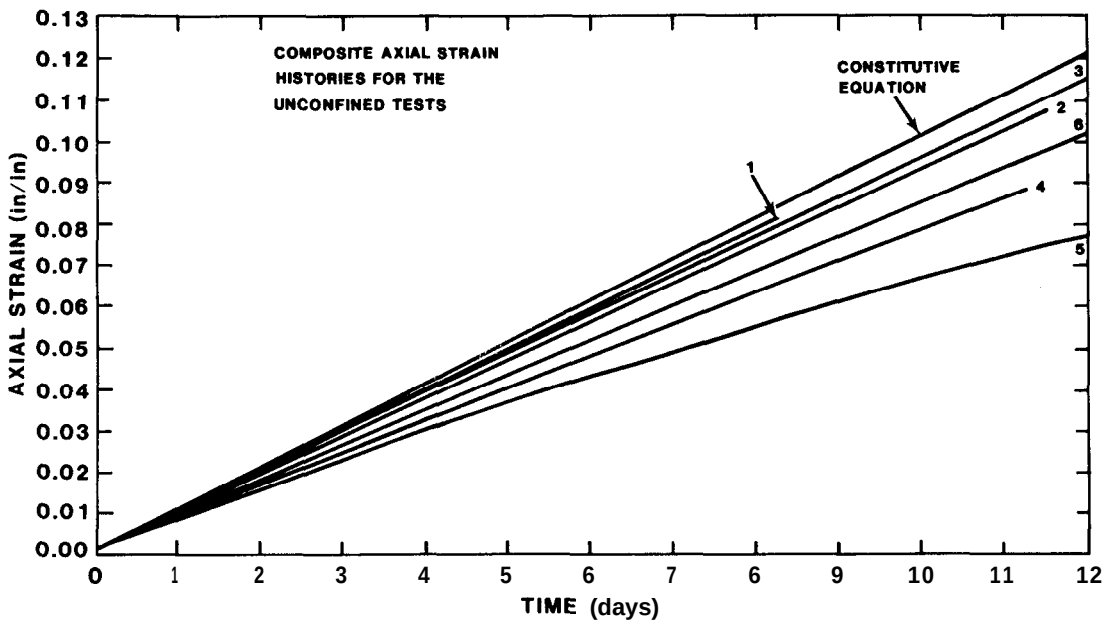

Figure 2. Axial Strain Versus Time For The Unconfined Test Simulations (see Table II for number code).

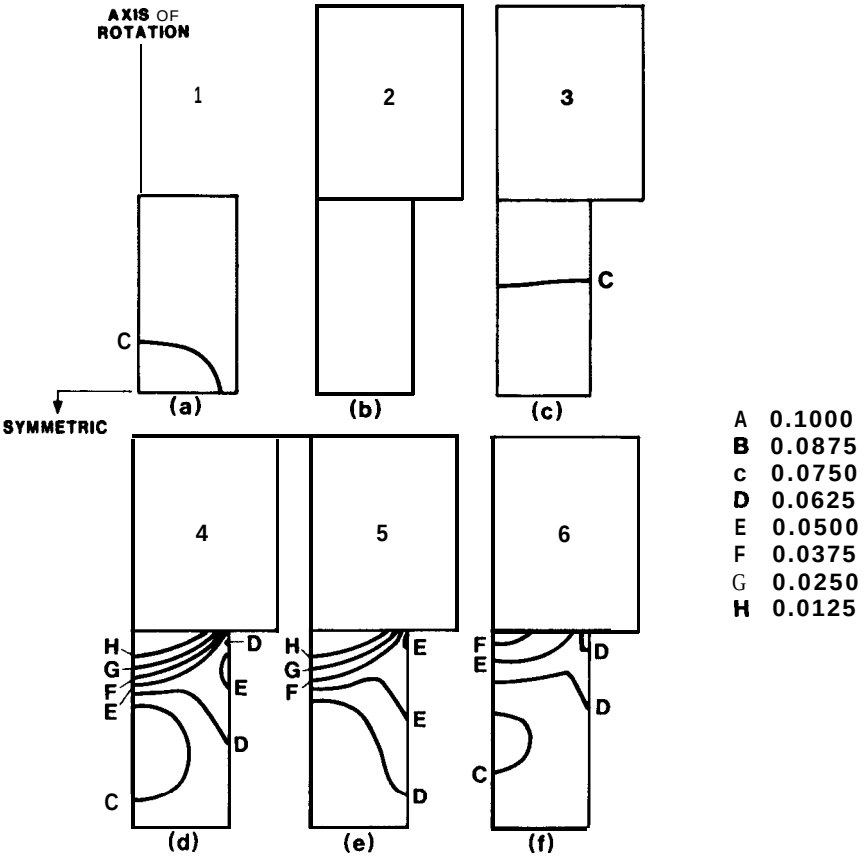

Figure 3. Axial Strain Contours At Eight Days For The Unconfined Test Simulations (see Table II for number code).

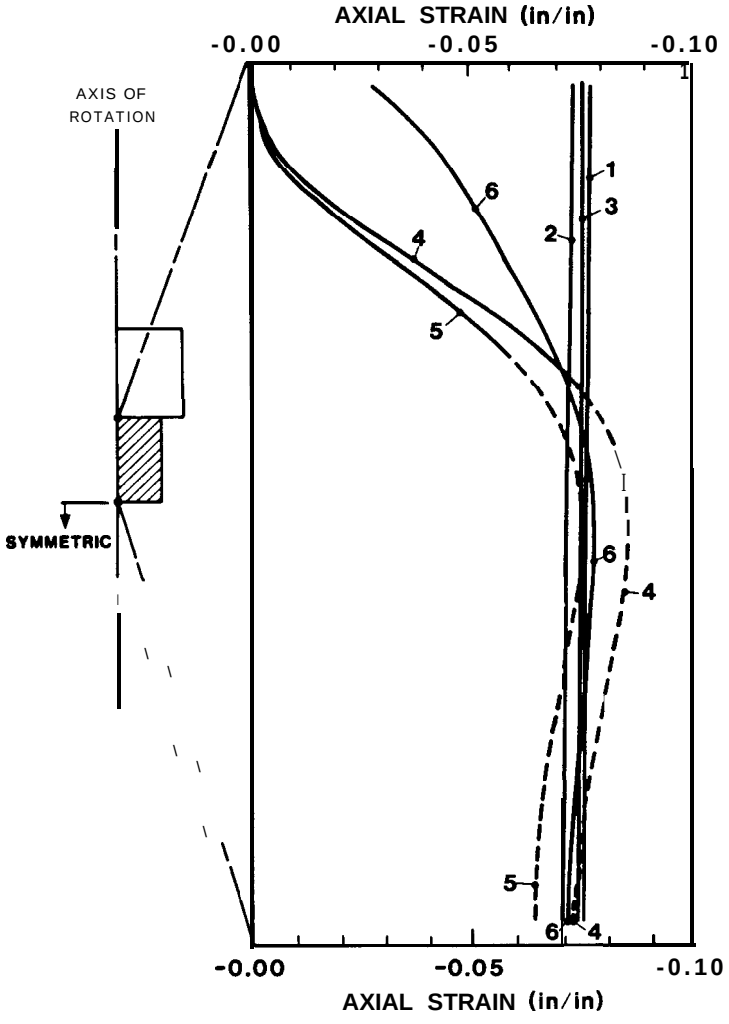

Figure 4. Axial Strain Profiles Along the Specimen Axis For the Unconfined Test Simulations at Eight Days (see Table II for number code).

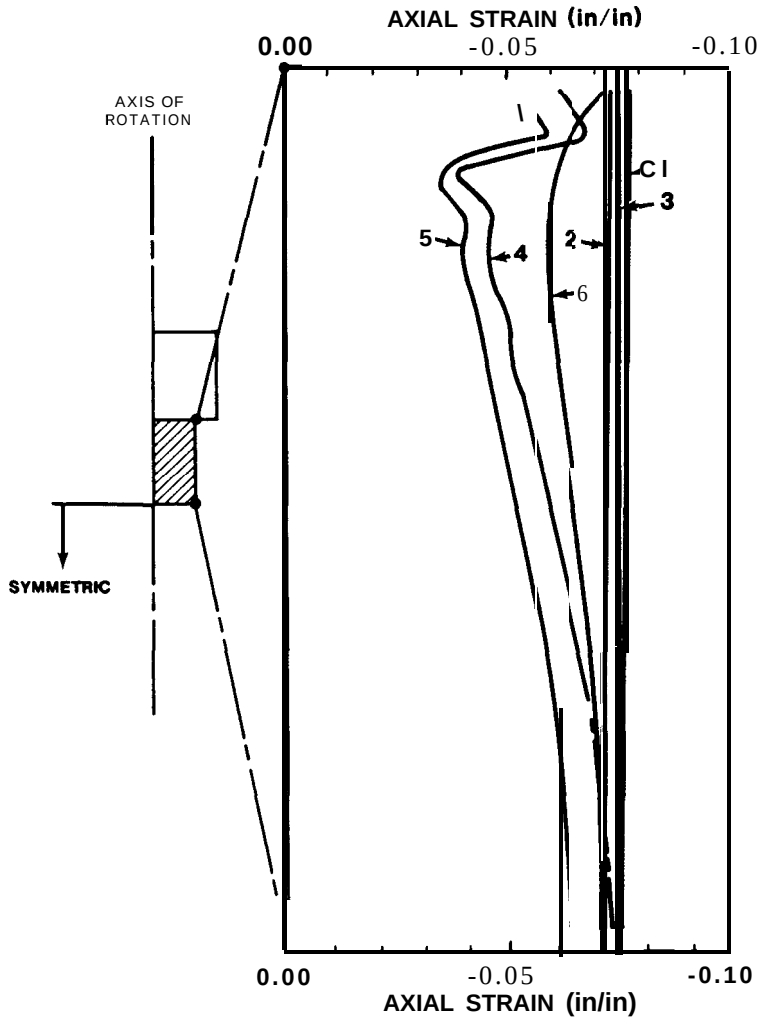

Figure 5. Axial Strain Profiles Along the Specimen Surface For the Unconfined Test Simulations at Eight Days (see Table II for number code).

axial strains for Simulations 2 and 2' were 0.0740 and 0.0734, respectively. Thus, the manner in which the steel platen is loaded appears to have very little influence on the predicted behavior. This agrees with the results of Baligh (1973) for relatively "stiff" platens applied to hard rock specimens. Simulation 2 behaves very similarly to Simulation 1 as shown in Figures 3 through 5.

Simulation 3 was performed to identify the importance of the convergence tolerance. An arbitrarily small convergence tolerance is impossible to achieve, for numerical as well as economic reasons. This simulation was performed with a convergence tolerance which was too expensive to use for all calculations. It is seen that the predicted results are sensitive to the convergence tolerance used, but also that predicted deviations from the creep model (Equation 4) are reduced for more restrictive tolerances. Average axial strain in Simulation 3 is 5.32 percent below the creep model at 8 days, with a value of 0.0766. Comparing Simulations 2' and 3, lowering the convergence tolerance from 0.5 percent to 0.3 percent (a reduction to 0.6 of the previous value) caused a factor of 1.74 decrease in the percent deviation from the creep model at 8 days. At 8 days, Simulation 2' has 0.0032 less axial strain than Simulation 3, a reduction of 4.13 percent. This effect is due entirely to the difference in the convergence tolerance. Therefore it is postulated that the deviation of average axial strain from the creep model calculated for all of the other unconfined simulations except Simulation 3 are on the high side by a minimum factor of 2 (minimum because further reductions in the convergence tolerance are expected to further reduce the deviation).

This observation implies that the idealized Simulation 1 may only deviate from the creep model by a maximum of two percent. This remaining error could be due to non-exact integration of the creep equation within the finite element code, the need for further reduction in the equilibrium convergence tolerance, or other factors. Further discussions of the percentage deviations in average axial strain from the creep model or between test simulations will not account for the possible factor of 1.74 or more to be gained by a more restrictive convergence tolerance.

The effect of a completely fixed interface may be seen in Simulation 4, where the convergence tolerance was restored to the more easily solved 0.5 percent. Figure 2 indicates that the effect is substantial. This is further shown in Figure 3. As contrasted to the fairly uniform axial strain state of the first simulations, a highly nonuniform state of axial strain is apparent. Near the top of the specimen at the axis, tne axial strain is greatly reduced. Further investigation showed that this is an area of reduced effective stress due to the fixed interface. This effect was also seen by Baligh (1973) in hard rock, and is often referred to as a conical dead zone. The degree of unloading, as well as the variation of axial strain along the length of the 'specimen on its axis and surface is seen in Figures 4 and 5, respectively. At eight days, Simulation 4 shows 23.26 percent less axial strain than the creep model, with an average axial strain of 0.0621. A comparison between Simulations 4 and 2' shows that varying the interfacial friction coefficient from perfect slip to complete bonding causes the percentage reduction from the creep model at 8 days to vary by 14 percent.

Along the axis and slightly below midheight of the specimen in Simulation 4 is the only location where axial strain is observed to exceed the theoretical value of 0.0809 (refer to Figure 4). The wavy behavior seen in the surface profile plot (Figure 5) near the specimen-platen interface is most likely a numerical anomaly and not real. Baligh (1973) presented nondimensionalized plots of the same kind as shown in Figures 4 and 5 for hard rock, and showed analogous behavior.

Simulation 5 shows that the force update procedure has a large effect on axial strain behavior (refer to Figures 2 through 5). Simulation 5 was identical to Simulation 4 except for the removal of this procedure, and showed an 8 day axial strain of only 0.0540. Thus,simulation 5 is 33.25 percent below the creep model at 8 days, an error increase of 10 percent from Simulation 4. Although this simulation was of no value in investigating the effect of interfacial friction on induced end effects, or in evaluating the effects of numerical parameters such as the convergence tolerance, it was of interest for developing an overall feel for the importance of different possible variables in the modeling of such tests.

The final unconfined uniaxial test simulation was an attempt to model a realistic laboratory experiment, with an interface friction coefficient of 0.15. Simulation 6 also had the force update and used a 0.5 convergence tolerance. As expected, the deviation in average axial strain from the creep model is intermediate between cases with zero friction and a perfectly bonded interface (refer to Figures 2 through 5). Simulation 6 is 16.74 percent below the creep model axial strain at 8 days, with an average axial strain of 0.0674. A comparison of Simulation 6 to Simulation 2' shows that a change from a zero interfacial friction coefficient to a realistic value causes the reduction in 8 day

overall axial strain from the creep model to be multiplied by a factor of 1.81. Simulation 6 was continued to large values of axial strain, so that some idea of deviation from the creep model at such strains could be determined. The results will be described in the next section along with results of Simulation 7, the confined test simulation.

LARGE STRAIN RESULTS

Triaxial creep tests may be taken to strains of 0.20 or more when multistage testing is being performed on one specimen. Therefore, the unconfined test (Simulation 6 in Table II) and the confined test (Simulation 7 in Table II) were both analyzed to axial strains greater than 0.18. The axial strain versus time results are shown in Figure 6 for the unconfined analysis and Figure 7 for the confined analysis, and compared to the creep model (Equation 4) in each case. As was shown in Figure 2, including friction at the salt/steel interface introduces a larger discrepency between the computed axial creep strain and the results of Equation 4 than would be seen in the frictionless case. In this case the difference between the theoretical strain (Equation 4) and the simulations at an axial strain of 0.17 is 19 percent for the unconfined analysis and 33 percent for the confined analysis. The difference in strain rate between the analysis and the creep model at an axial strain of 0.17 is 23.5 percent for the unconfined analysis and 32 percent for the confined analysis.

The results of the confined analysis may include some error induced by the convergence procedure used. Due to the finite friction slip plane and the presence of the radial confining pressure, this analysis was exceptionally slow to converge at the usual tolerance of 0.5 percent. For this reason the tolerance was relaxed after the axial strain had reached one percent so that when the equilibrium parameter was less than 1.3 percent after 300 iterations, the step was prematurely terminated and the solution was continued. Unconfined Simulation 3 showed that if held constant throughout the analysis, the value of the convergence tolerance is an important parameter in determining the deviation from the creep model. The deviation from the creep model was seen in Simulation 3 to be reduced for smaller convergence tolerances, however.

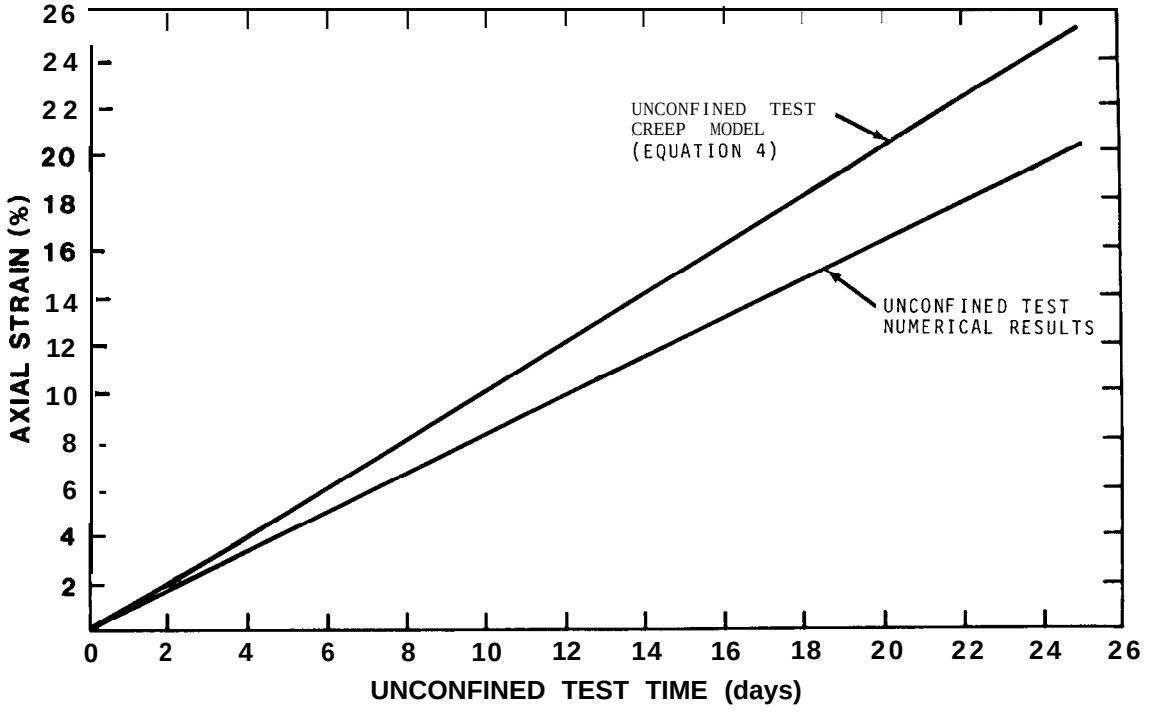

Figure 6. Axial Strain Versus Time For Unconfined Test Simulation 6 With Realistic Interfacial Friction, Out to Large Strains.

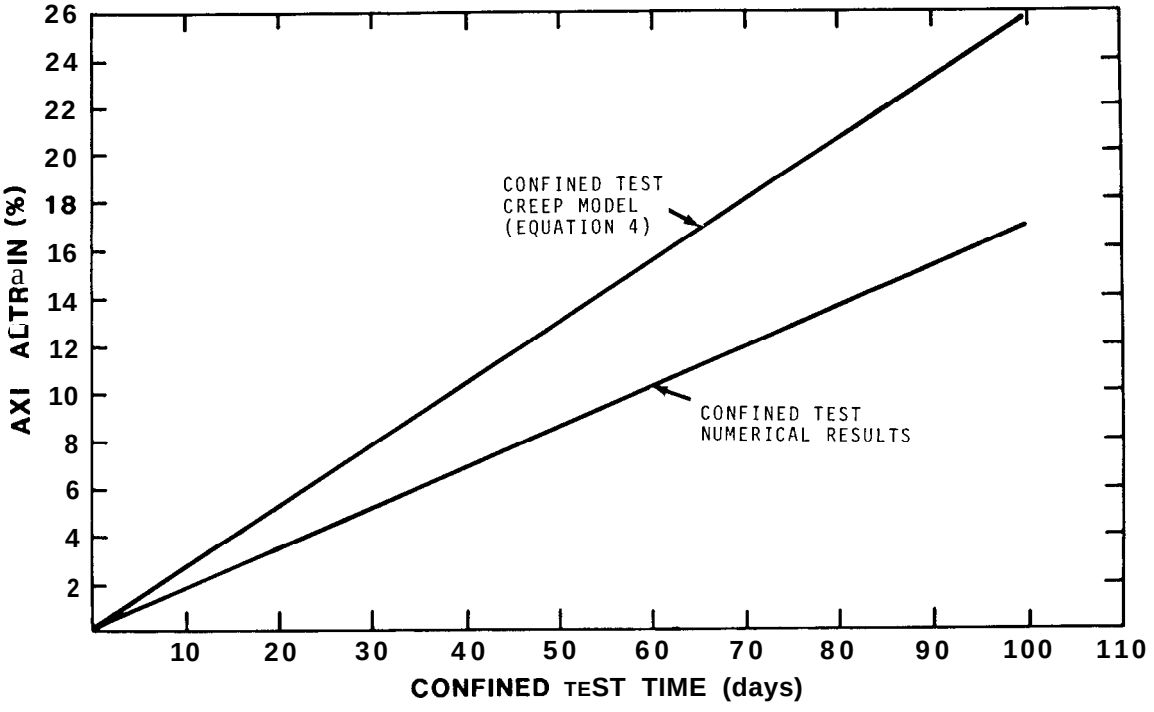

Figure 7. Axial Strain Versus Time For the Confined Test Simulation 7 Out to Large Strains.

The computed axial strain is shown in Figure 8 along the specimen axis and on the specimen surface for a nominal axial strain of 17 percent, for both Simulation 6 and Simulation 7. In both simulations the axial strain tends to zero on the axis at the salt/steel interface and increases significantly above the nominal strain along the axis approximately half of the distance between the interface and the specimen midheight. Inversely for locations on the specimen surface, an axial strain concentration well above the nominal value occurs at the top interface in both simulations. The surface axial strain then goes to reduced values just below the interface, gradually increasing as the specimen midheight is approached. On the midplane of the specmen, a relatively uniform axial strain state near the nominal value is evident. Baligh (1973) noted very similar behavior near the surface of rock specimens in triaxial compression.

Contours of axial strain in each specimen at 17 percent nominal strain are shown in Figure 9. The contours clearly show the conical dead zone similar to the other unconfined test simulations and Figure 8.

AXIAL STRAIN RATES

Axial strain rate, as well as average axial strain, is a quantity of interest when evaluating end effect inhomogeneities in triaxial creep tests. A summary of axial strain rate for each of the unconfined test simulations at an average axial strain value of 0.07 is presented in Table III. Also included in the table are the axial strain rates for the unconfined Simulation 6 and the confined Simulation 7 at an average axial strain of 0.17. Rates are given in average axial strain per day. Table III summarizes the percentage reduction in the given strain rates from the creep model (Equation 4) at the given axial strain values.

Errors in axial strain rate for the test simulations appear to be in the range seen for average axial strain, at low values of axial strain. In addition, there is some evidence that in an actual laboratory creep test, strain rate errors may increase at higher values of average axial strain.

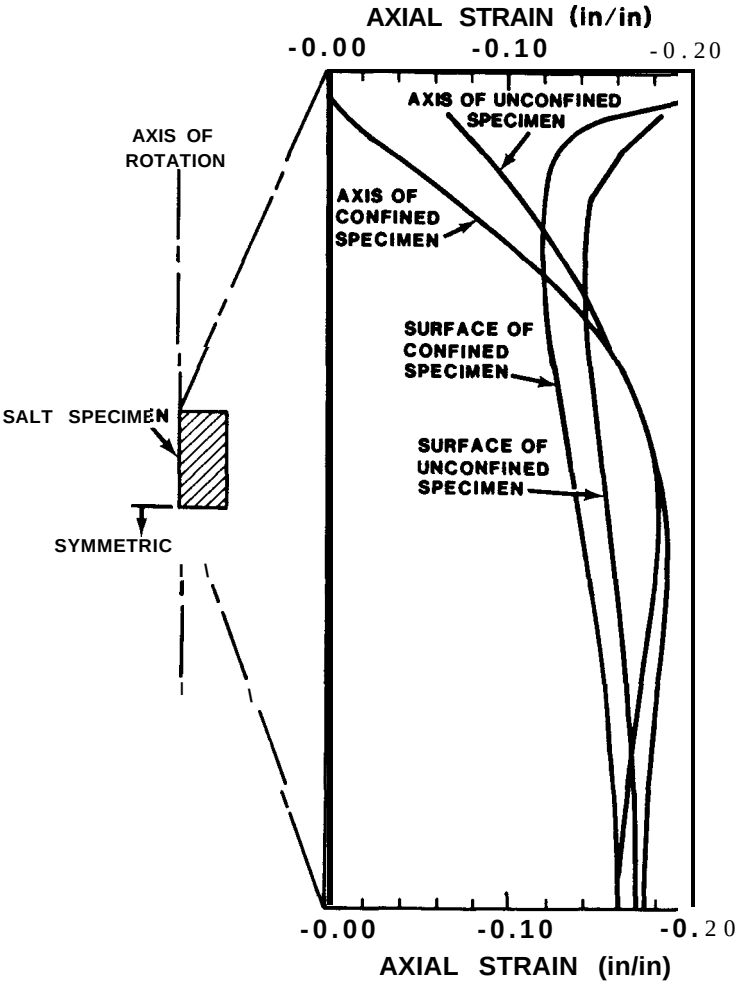

Figure 8. Axial Strain Profiles Along The Specimen Axis at 17 Percent Axial Strain.

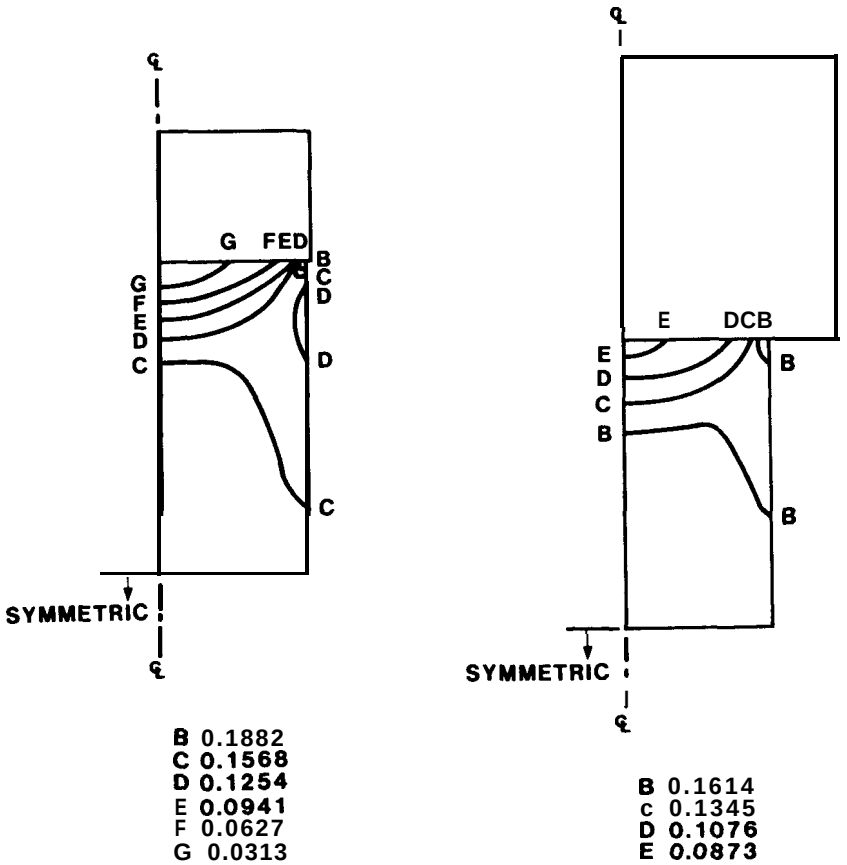

Figure 9. Axial Strain Contours For the Confined and Unconfined Test Analyses At 17 Percent Axial Strain.

Table III. Average Axial Strain Rate (l/day), and Percentage Strain Rate Reduction from Creep Model, at Specified Average Axial Strain Values.

SIMULATION	AVERAGE AXIAL STRAIN RATE AT AVERAGE AXIAL STRAIN OF 0.07 (1/day)	PERCENTAGE STRAIN RATE REDUCTION FROM CREEP MODEL (%)	AVERAGE AXIAL STRAIN RATE AT AVERAGE AXIAL STRAIN OF 0.17 (1/day)	PERCENTAGE STRAIN RATE REDUCTION FROM CREEP MODEL (%)
1	0.99	2.0		
2	0.92	8.75		
3	0.95	5.75	- -	——
4	0.76	24.4		- -
5	0.54	46.3		
6	0.82	18.5	0.77	23.5
7			.175	32

SUMMARY

A parametric study involving six simulations of unconfined uniaxial tests on rock salt specimens, as well as a single simulation of a more complex confined test, were performed. Deviation of computed axial strain from a theoretical creep model was studied. Computed axial strain was below the creep model in every case. One reason for this lies in the numerical analysis and the economic constraint preventing an arbitrarily small convergence tolerance for the dynamic relaxation procedure. It was shown that changing the tolerance from 0.5 percent to 0.3 percent could reduce the difference between the creep model and the predicted strain rates from 8.75 percent to 5.75 percent at eight days (see Table III). The strain rate was increased from .92 to .95 percent per day. The second reason the numerical results are below the creep model is the inhomogeneities in the stress and strain fields in the specimen, the determination of which was the main purpose of this study. It was shown that interfacial friction ranging from perfect slip to complete bonding caused a 15.7 percent change in the axial strain rate compared to that predicted by the creep model at eight days. The percent reduction in axial strain rate from the creep model was multiplied by a factor of 2.11 at eight days when interfacial friction was changed from perfect slip to a realistic value of 0.15. It is likely that the nonhomogeneities caused by frictional end effects in actual experirnents cause errors on the order of 10 percent in both the axial strain and the strain rate when overall sample strain is about 8 percent. The error in both axial strain and strain rate also increases with increasing strain being somewhere around 20 percent when the the axial strain is about 0.20.

These preliminary results indicate that further study is needed to better understand the triaxial creep test procedure and the determination of creep models from these tests. Further numerical studies may indicate ways in which the force update procedure may be improved and the interpretation of the creep data enhanced to minimize the error due to end effects.

REFERENCES

Brady, B. T. ,1971, The Effect of Confining Pressure On The Elastic Stress Distribution in a Radially End-Constrained Circular Cylinder, International Journal of Rock Mechanics, Vol 8, pp 153-164, Pergamon Press.

Baligh, Mohsen M., 1973, Numerical Study of Uniaxial and Triaxial Rock Compression Tests, Systems, Science and Software, SSS-R-1658, La Jolla, Calif.

Herrmann, W., Wawersik, W. R., Lauson, H., 1980, Analysis of Steady State Creep of Southeastern New Mexico Bedded Salt, Sandia National Laboratories, SAND-80-0558.

Malvern, Lawrence E., 1969, Introduction to the Mechanics of a Continuous Medium, Prentice-Hall, Inc. , Englewood Cliffs, New Jersey.

Peng, S. D., 1971, Stresses Within Elastic Circular Cylinders Loaded Uniaxially and Triaxially, International Journal of Rock Mechanics, Vol 8, pp 399-432, Pergamon Press.

Wawersik, Wolfgang R., Hannum, David W., Lauson, Hank S., 1980, Compression and Extention Data for Dome Salt from West Hackberry, Louisiana, Sandia National Laboratories, SAND79-0668.

Wawersik, W. R. and Preece, D. S., 1981 Creep Testing of Salt -- Procedures, Problems and Suggestions, First Conferance on the Mechanical Behavior of Rock Salt, Penn State University.

Weart, W. D.,1981, Reference Creep Law and Material Properties for WIPP, Letter to Distribution, Sandia National Laboratories, July,1981.